Journal of Industrial Microbiology & Biotechnology (2001) 26, 53–61

www.nature.com/jim

Potentials of radio-frequency field gradient NMR microscopy in environmental science

F Humbert

Laboratoire de Chimie Physique pour l'Environnement UMR 7564 — CNRS/Université H. Poincaré, Nancy I 405, rue de Vandoeuvre 54600 Villers-lès-Nancy, France

An understanding of transport, flow, diffusivity and mass transfer processes is of central importance in many fields of environmental biotechnology such as biofilm, bioreactor and membrane engineering, soil and groundwater bioremediation, and wastewater treatment. Owing to its remarkable sensitivity to molecular displacements and to its noninvasive and nondestructive character, pulsed field gradient (PFG) nuclear magnetic resonance (NMR) can be a valuable tool for investigating such processes. In conventional NMR microscopy, spatial encoding is achieved by using static magnetic field gradients (B_0 gradients). However, an interesting alternative is to use radio-frequency magnetic field gradients (RF or B_1 gradients). Although the latter are less versatile than the former, RF field gradient microscopy is particularly suitable for dealing with heterogeneous systems such as porous media because of its quasi-immunity to background static magnetic field gradients arising from magnetic susceptibility inhomogeneities, unlike the B_0 gradients microscopy. Here, we present an overview of basic principles and the main features of this technique, which is still relatively unused. Different examples of diffusion imaging illustrate the potentialities of the method in both micro-imaging and the measurement of global or local diffusion coefficients within membranes and at liquid–solid interfaces. These examples suggest that a number of environmental problems could benefit from this technique. Different future prospects of application of B_1 gradient NMR microscopy in environmental biotechnology are considered. *Journal of Industrial Microbiology & Biotechnology* (2001) **26,** 53–61.

Keywords: NMR microscopy; diffusion map; radio-frequency field gradients; NMR micro-imaging; membrane; localized diffusion coefficient

Introduction

An understanding of fluid-transport processes is of central importance to many investigations in environmental biotechnology. Thus, in biofilm and bioreactor engineering, investigation of mechanisms for transport of water, nutrients and antimicrobial agents within biofilms *via* measurement of local diffusion coefficients in the interstitial voids and in the cell clusters of heterogeneous biofilms [3,7,54,61] is of particular interest to know the biofilm structure and development [2,50] and to optimise bioreactors [13,49,55]. Soil and sediment bioremediation also needs knowledge of mechanisms responsible for the migration of pollutants (organic molecules [11,30,47], heavy metals [27,41]) and the influence of transport processes on the bioavailability of organic xenobiotics [20,43,56]. Wastewater treatment is another field in which transport processes are crucial (e.g., transport processes in granular sludge [36], characterisation of the floc structure and sedimentation [15], the hydration state of sewage sludges [32], and membrane filtration technology). To date, the most widely used methods in environmental sciences for studying transport processes are the fluorescence recovery after photobleaching (FRAP) technique possibly combined with confocal scanning laser microscopy [3], the limiting current technique and microelectrodes [61], tracer techniques and effluent breakthrough curves [51]. Another method of particular relevance for studying translational molecular diffusion is pulsed field gradient (PFG) nuclear magnetic resonance (NMR) [8,53]. As a noninvasive method, unlike the conventional methods, it allows observation of molecular displacements in the range 0.1–100 μm [44] without interfering with internal processes. Moreover, when combined with NMR imaging, localized velocity and self-diffusion coefficient maps can be obtained. Applied at high spatial resolution, this method is termed dynamic NMR microscopy [8]. These features make PFGNMR spectroscopy the method of choice not only for measuring diffusion coefficients (under favourable circumstances to less than 10^{-13} cm^2 s^{-1} [44]) of solutes in chemical and biological systems but also for probing the environment of diffusing molecules, for example, the size and permeability of cells in biological tissues [35,42] or the pore size in porous media [34]. However, this method is still relatively unused in environmental science. Only a few recent papers demonstrate that PFGNMR is a reliable method for studying the diffusion processes in sludges, biofilms and clays [4,36–38,40,57,60]. In conventional NMR microscopy, spatial encoding is achieved by using static magnetic field gradients ($\mathbf{B}_0$ gradients). However, in heterogeneous systems, magnetic susceptibility differences between different microregions, for example between a solid matrix and the pore fluid, can lead to substantial magnetic field gradients that interfere with externally applied field gradients. These susceptibility-induced gradients are called ''internal or background gradients'' and cause distortions in imaging and diffusion measurements [26]. Numerous methods [17,29,33,39,58] have been proposed to mitigate these harmful effects. They require very strong gradients [31,48] or sophisticated experimental techniques [18]. In addition, the

Correspondence: Dr F Humbert, Laboratoire de Chimie Physique pour l'Environnement, UMR 7564 — CNRS/Université H. Poincaré, Nancy I 405, rue de Vandoeuvre 54600 Villers-lès-Nancy, France
Received 9 February 2000; accepted 7 August 2000

efficiency of these methods depends strongly on the strength and nonuniformity of background gradients, on diffusion times, on the diffusion coefficient values and on the size of regions possessing different magnetic susceptibility [26]. To avoid problems related to background gradients, an alternative of choice is to use radio-frequency field gradients ($\mathbf{B}_1$ gradients). Indeed this technique is quasi-insensitive to magnetic susceptibility differences within the object under investigation [46]. Furthermore, its experimental set-up is relatively simple.

The aim of this paper is to review the basic principles and the main features of $\mathbf{B}_1$ gradient NMR microscopy. Some examples recently obtained in diffusion imaging will highlight the potentialities of the technique in both micro-imaging and diffusion measurements and will show that $\mathbf{B}_1$ field gradient NMR microscopy could be a valuable tool in environmental science.

Spatial encoding in NMR microscopy: $\mathbf{B}_0$ and $\mathbf{B}_1$ gradients

NMR is a spectroscopy based on interactions between the magnetic moment $\boldsymbol{\mu}$ associated with a nucleus with nonzero spin (e.g., ^{1}H, ^{13}C, ^{31}P) and two applied magnetic fields: (i) a static magnetic field $\mathbf{B}_0$ (a few tesla) whose direction defines the Z axis and which is continuously generated by an electromagnet or a superconducting magnet and (ii) a radio-frequency (RF) magnetic field of amplitude B_1 (10^{-4} tesla) oscillating at a frequency ν_1 and applied perpendicularly to $\mathbf{B}_0$ as short bursts (or pulses) by passage of an RF current through a coil whose axis is usually assigned as the X direction. The former field polarises nuclear spins, thus creating distinct energy levels and the latter induces transitions among these energy levels. The transition (or resonance) frequency is dependent on the magnetic field amplitude B_0 according to the formula:

$$\nu_0 = \gamma B_0/2\pi \quad (1)$$

where γ is the gyromagnetic ratio of the nuclei under investigation. To understand many of the experimental aspects of NMR microscopy, it is often sufficient to consider the evolution of the magnetisation $\mathbf{M}$, which is the sum of the nuclear magnetic moments $\boldsymbol{\mu}$, in the presence of the fields $\mathbf{B}_0$ and $\mathbf{B}_1$. At thermal equilibrium, the magnetisation $\mathbf{M}$ is aligned with $\mathbf{B}_0$ and no signal is detected. However, if a secondary magnetic field $\mathbf{B}_1$ is generated orthogonal to $\mathbf{B}_0$ by application of an RF pulse, then, according to classical mechanics, the interaction of the fields $\mathbf{B}_0$ and $\mathbf{B}_1$ with $\mathbf{M}$ causes $\mathbf{M}$ to precess simultaneously about $\mathbf{B}_0$ and $\mathbf{B}_1$, respectively, at the Larmor frequency equal to the resonance frequency ν_0 given by Equation 1 and at the nutation frequency ν_1 given by:

$$\nu_1 = \gamma B_1/2\pi \quad (2)$$

The phenomenon is illustrated in Figure 1. Viewed in the frame rotating with frequency ν_1 about the $\mathbf{B}_0$ direction, the motion is simply a precession about $\mathbf{B}_1$ at the frequency ν_1. After the pulse, $\mathbf{M}$, only subjected to $\mathbf{B}_0$, precesses about $\mathbf{B}_0$ at the Larmor frequency. The precession of transverse magnetization $\mathbf{M}_{XY}$ produces a detectable signal (the NMR signal) by inducing an RF current at frequency ν_0 in the coil situated in the XY plane. For more details see Ref. [8]. Now, according to Equation 1, if by means of specially shaped coils a spatially dependent magnetic field gradient $\mathbf{g}_0$ is superimposed onto $\mathbf{B}_0$, ν_0 becomes spatially dependent:

$$2\pi\nu_0(\mathbf{r}) = \gamma B_0 + \mathbf{g}_0 \cdot \mathbf{r} \quad (3)$$

Thus the Larmor frequency of the nuclear spins differ from one location to another across the sample. This simple linear relation

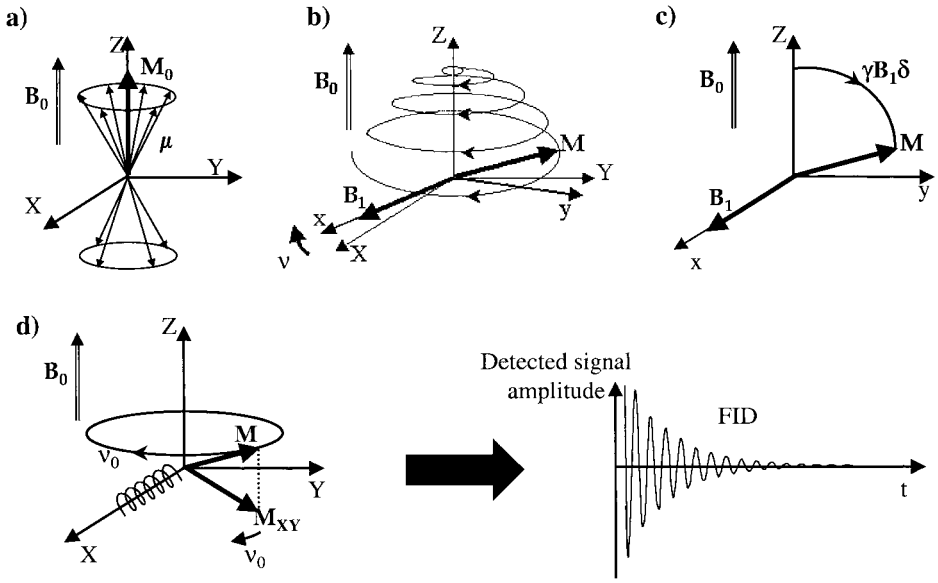

Figure 1 Vector description of nuclear magnetization $\mathbf{M}$ in the presence of a static magnetic field $\mathbf{B}_0$ and a radio-frequency (RF) magnetic field $\mathbf{B}_1$. (a) Excess spin population (for spin 1/2) aligned with $\mathbf{B}_0$ resulting in a net magnetization in the Z direction. (b) Evolution of $\mathbf{M}$ in the laboratory frame in the presence of the fields $\mathbf{B}_0$ and $\mathbf{B}_1$. When the frequency ν is equal to the Larmor frequency ν_0 $\mathbf{M}$ simultaneously precesses about $\mathbf{B}_0$ at ν_0 and about $\mathbf{B}_1$ at ν_1. (c) As for (b) but in the rotating frame where $\mathbf{B}_1$ is stationary. Only the precession about $\mathbf{B}_1$ is apparent. (d) Following excitation by an RF pulse the precession of the transverse magnetization $\mathbf{M}_{XY}$ about $\mathbf{B}_0$ induces an RF current in a receiver coil situated in the XY plane: it is the NMR signal. Fourier transformation of signal in the time domain (free induction decay: fid) produces the NMR frequency spectrum.

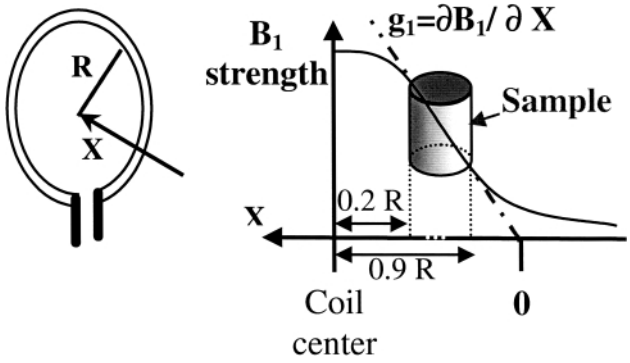

Figure 2 Schematic representation of the profile of the radio-frequency field produced by a single-turn coil. The $\mathbf{B}_1$ gradient is constant in the range from 0.2 to 0.9 R.

between the Larmor frequency and the nuclear spin coordinates, **r**, lies at the heart of the spatial encoding technique in conventional NMR microscopy. In the same way, if an RF magnetic field gradient $\mathbf{g}_1$ is superimposed onto $\mathbf{B}_1$, then the nutation frequency becomes spatially dependent:

$$2\pi\nu_1(\mathbf{r}) = \gamma \mathrm{B}_1 + \mathbf{g}_1 \cdot \mathbf{r} \qquad (4)$$

In comparison with $\mathbf{B}_0$ gradients, the use of $\mathbf{B}_1$ gradients is relatively recent. Hoult [19] was the first to propose in 1979 an imaging method based on both $\mathbf{B}_0$ and $\mathbf{B}_1$ gradients in order to overcome some problems related to $\mathbf{B}_0$ gradient switching (in particular, difficulties in obtaining gradient pulses with very rapid rise and fall times and in controlling the eddy currents induced in the surrounding metal parts of the probe; these difficulties do not exist with $\mathbf{B}_1$ gradients). As for diffusion measurements, the first study performed with $\mathbf{B}_1$ gradients was reported by Karczmar in 1988 [28]. Nevertheless, difficulties in generating large $\mathbf{B}_1$ gradients and creating two or three independent orthogonal $\mathbf{B}_1$ gradients have limited the development of this technique. In spite of these drawbacks, important instrumental advances made by the $\mathbf{B}_0$ gradient technique over the last years and the popularity of the latter, $\mathbf{B}_1$ gradients retain a valuable asset, namely, a quasi-insensitivity to magnetic susceptibility variations across the sample due to the B_1 amplitude that is several orders of magnitude smaller than the B_0 amplitude. Consequently, $\mathbf{B}_1$ gradient NMR microscopy is particularly suited for studying diffusion processes in heterogeneous systems (such as porous media [12]) that are frequent in environmental science.

Basic principles of RF field gradient NMR microscopy

RF field gradient NMR microscope probe: Among the various approaches proposed for producing $\mathbf{B}_1$ gradients, the single-turn coil has proved to be the most effective device. In addition to its instrumental simplicity, the major advantage of such a device stems from its capability of delivering a uniform $\mathbf{B}_1$ gradient in a region ranging from $0.2R$ to $0.9R$ where R is the coil radius [1,10,16] (Figure 2). However, as mentioned above, for a long time this technique has suffered from difficulties associated with producing large uniform $\mathbf{B}_1$ gradients. It must be borne in mind that the stronger the gradients, the higher the spatial resolution and the wider the measurable diffusion coefficient range. Fortunately, over the last 4 years, a significant advance, opening new prospects, has been the development of RF gradient probes delivering relatively large constant $\mathbf{B}_1$ gradients, up to 100 G cm^{-1}, and operating at frequencies ranging from 10 to 300 MHz [21,22]. Such a probe is schematized in Figure 3. It includes a flat concentric two-turn coil generating the $\mathbf{B}_1$ gradient and a Helmholtz or saddle coil (according to the magnet type) for collecting the NMR signal and producing homogeneous pulses. The gradient strength depends directly on the quality factor of the resonant circuit, the RF power, the coil radius, and the RF frequency. With such a device, Equation 4 can be rewritten in the form:

$$2\pi\nu_1(X) = \gamma \mathbf{g}_1 X \qquad (5)$$

by defining the X axis as the $\mathbf{B}_1$ gradient direction.

Diffusion experiment: An intuitive understanding of the principle of diffusion measurements using $\mathbf{B}_1$ gradients can be

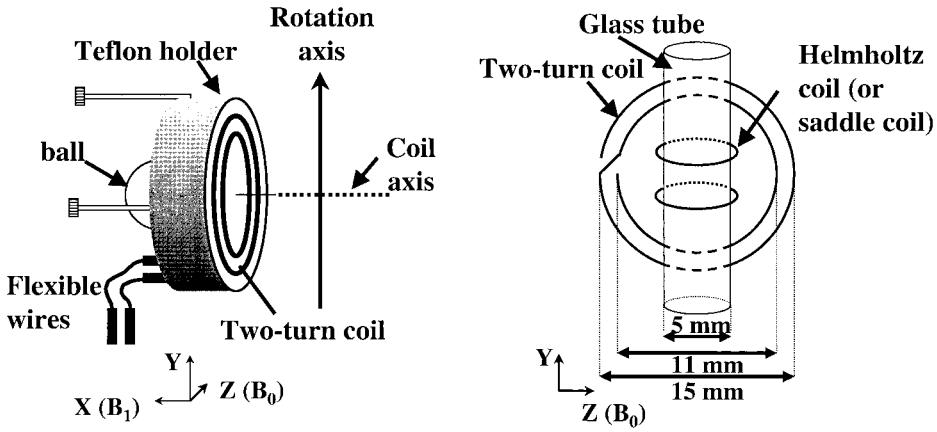

Figure 3 Schematic view of the radio-frequency field gradient NMR microscope probe delivering $\mathbf{B}_1$ gradient up to 110 G cm^{-1} and operating at frequencies ranging from 10 to 300 MHz. The flat concentric two-turn coil generates the $\mathbf{B}_1$ gradient and a Helmholtz or saddle coil (according to the magnet type) collects the NMR signal and produces homogeneous pulses. At 90 MHz and with an RF power of 275 W the RF field amplitude ranges from 17 G to 35 G across the sample. The different mechanical parts (Teflon holder, ball, flexible wires, etc.) minimize electric coupling between the two coils and allow adjustment of the region where the $\mathbf{B}_1$ gradient is constant.

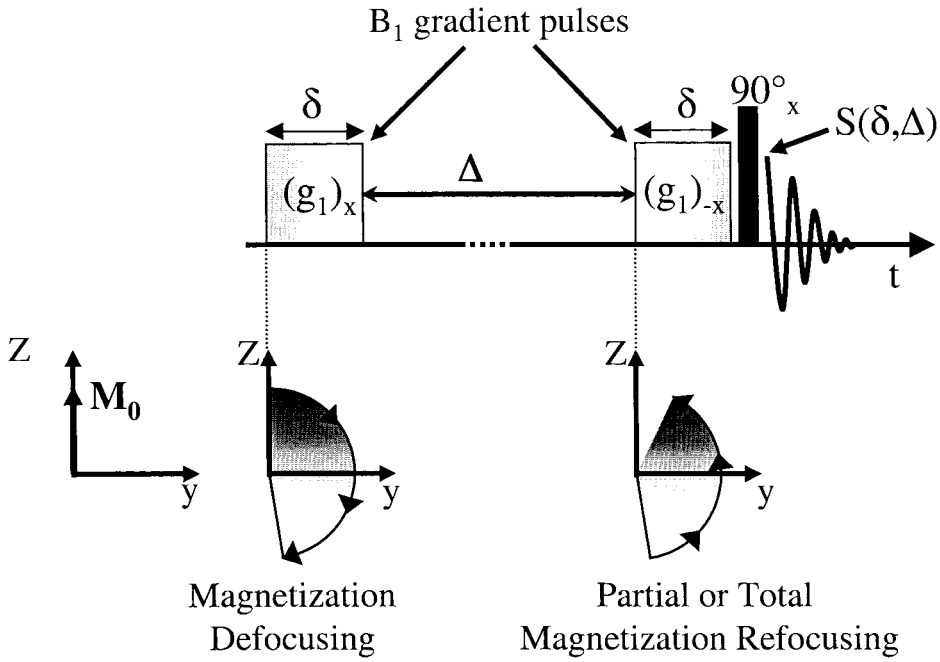

Figure 4 Basic sequence for studying translational molecular motion with radio-frequency field gradients and magnetization evolution. The black rectangle represents a homogeneous pulse; Δ is the diffusion interval.

gained from Figure 4. According to Equation 5, the nutation angle generated by an RF field gradient pulse of length δ is spatially dependent:

$$\alpha(X) = \gamma \mathbf{g}_1 X \delta \tag{6}$$

Consequently a gradient pulse applied along the x axis of the rotating frame will cause a defocusing of the nuclear magnetization in the yZ plane. However, this defocusing process can be reversible. Indeed, if immediately afterwards, a second gradient pulse of identical duration but opposite phase (i.e., along $-x$) is applied, the magnetization is refocussed along the Z axis. A rotary echo is generated [52]. Now, if a period Δ is inserted between the two gradient pulses, the refocusing process may be incomplete due to translational molecular motions. Indeed, if molecular displacement occurs during Δ, the X coordinates of the individual spins at the time of the second gradient pulse will differ from those during the first pulse, hence a difference between nutation angles generated by the two gradient pulses. Thus, the diffusive movement leads to a net decrease of the detected signal after the $\pi/2$ read pulse. In the case of unrestricted diffusion, for a sample with a single resonance line, the signal amplitude S is given by [14]

$$S(\delta, \Delta) = \frac{\mathrm{M}_0}{2} \exp\left(\frac{-2\delta}{T_{12}}\right) \exp\left(\frac{-\Delta}{T_1}\right) \times \exp\left(-\gamma^2 \mathrm{g}_1^2 \delta^2 D \left[\Delta + \frac{2\delta}{3}\right]\right) \tag{7}$$

where M_0 is the magnitude of the equilibrium magnetization; T_1 is the longitudinal relaxation time; T_{12} is the time constant characterizing relaxation during the RF pulses; D is the self-

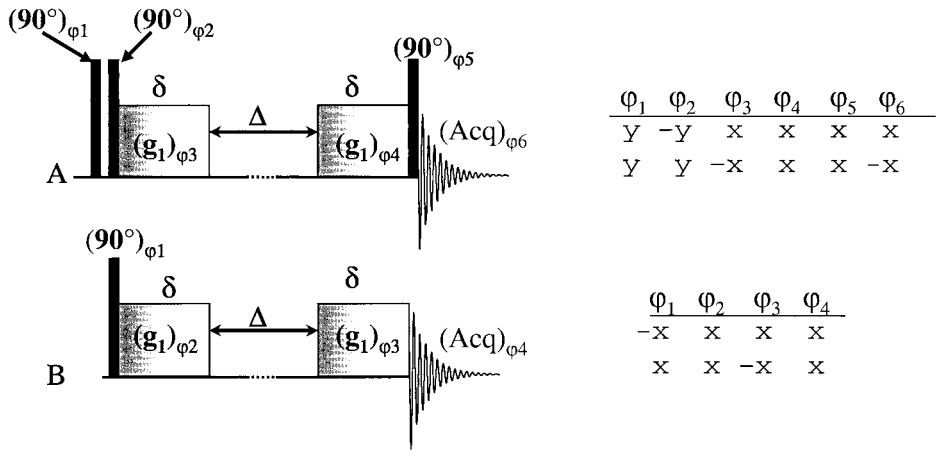

φ1	φ2	φ3	φ4	φ5	φ6
y	-y	x	x	x	x
y	y	-x	x	x	-x

φ1	φ2	φ3	φ4
-x	x	x	x
x	x	-x	x

Figure 5 Improved pulse sequence composed of the two subsequences A and B and their associated phase cyclings for diffusion measurements with RF field gradients.

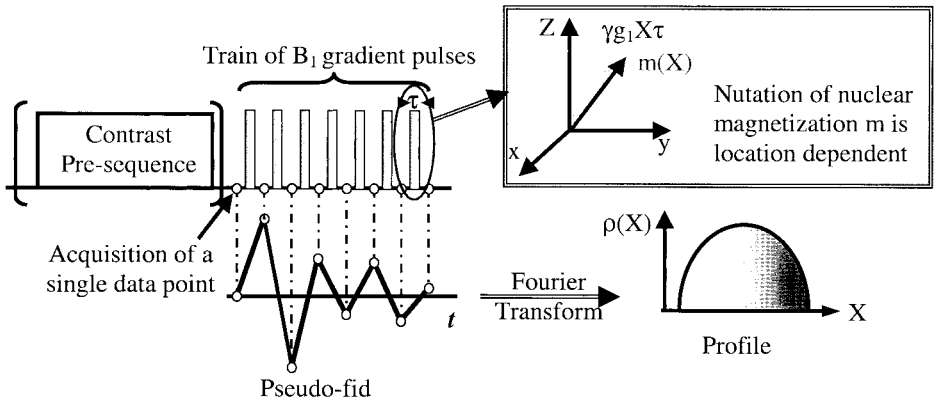

Figure 6 Rapid rotating frame imaging sequence. With an RF power of 275 W, typical values of τ and the period between the pulses are 3 and 50 μs, respectively. The data points so acquired constitute a pseudo-fid whose Fourier transform provides the spin density along the spatial gradient direction X. Various contrast schemes (in relaxation time, chemical shift, molecular motion) applied prior to the imaging step allow contrast profiles. The reconstruction of a two-dimensional image requires one to perform N rotations at regular angular intervals (typically 3.6°) and to record a profile for each new orientation. Subsequently, the images are reconstructed through the filtered-back-projection algorithm from the series of profiles.

diffusion coefficient. Neglecting the relaxation during RF pulses and setting $\Delta >> 2\delta/3$, expression (7) becomes:

$$S(\delta,\Delta) = \frac{M_0}{2}\exp\left(\frac{-\Delta}{T_1}\right)\exp\left(-\gamma^2 g_1^2 \delta^2 D\Delta\right) \qquad (8)$$

Nevertheless, a detailed assessment [24] of this simple sequence reveals that under some circumstances (small and/or heterogeneous samples, weak diffusion coefficients, very short relaxation times) the quality of measurements may be affected by a number of artifacts. To suppress these artifacts, it is necessary to use the more refined sequence sketched in Figure 5. We have demonstrated that this sequence allows the study of numerous types of diffusion processes ranging from rapid diffusion in the gas phase ($1\ cm^2\ s^{-1}$) to very slow diffusion ($10^{-9}\ cm^2\ s^{-1}$) in, e.g., surfactant systems, cells, membranes and other porous media [12,24,59].

Imaging experiment: In $\mathbf{B}_1$ gradients NMR microscopy, the basic imaging sequence consists of applying a train of $\mathbf{B}_1$ gradient pulses each of duration τ and acquiring a data point between two consecutive pulses [6] (Figure 6). This imaging method is called rapid rotating frame imaging. Considering the detected signal results from the precession of the transversal component of nuclear magnetization, the NMR signal detected following the 1th gradient pulse is

$$S(l\tau) = \int \rho(X)\sin(\gamma \mathbf{g}_1 X l\tau)dX \qquad (9)$$

where $\rho(X)$ is the spin density at abscissa X. The whole data set appears as a pseudo-fid (fid: free induction decay) whose Fourier transform represents the projection of the spin density upon the X direction. Because the $\mathbf{B}_1$ gradient is only applied along one direction, the reconstruction of a two-dimensional image requires to perform N rotations at regular angular intervals (typically 3.6°) and to record a profile for each new orientation. This necessity of rotating the sample for reconstructing a two-dimensional image is the weakness of the method essentially because this is time consuming. In $\mathbf{B}_1$ gradient imaging an in-plane spatial resolution in the order of a few micrometers can be achieved with gradient strength of 75 G cm^{-1} [21]. It is important to note that this spatial

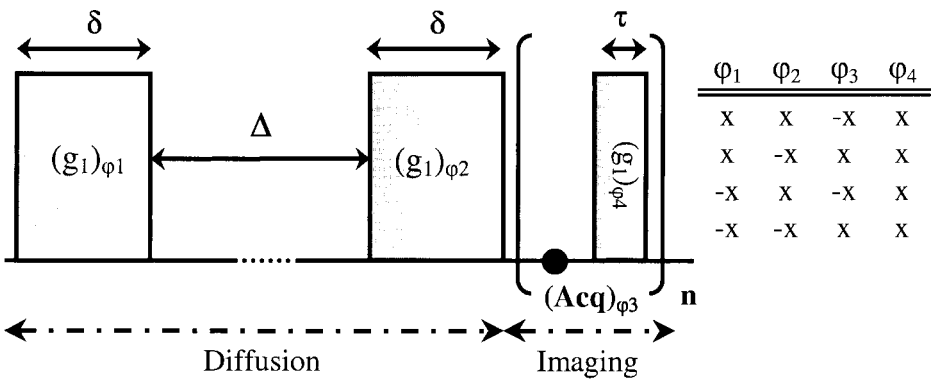

Figure 7 The basic sequence and the associated phase cycling for determining spatially resolved diffusion coefficients with RF field gradients. The first part (diffusion contrast period) with two $\mathbf{B}_1$ gradient pulses of duration δ and magnitude g_1 separated by a diffusion interval Δ, produces a decrease of longitudinal magnetization according to translational diffusion. Subsequently, in the second part, the z magnetization is spatially labelled by rapid rotating frame imaging. Fourier transform of the pseudo-fid provides a one-dimensional profile not only weighted by self-diffusion coefficient and T_1 but also unfortunately spatially modulated.

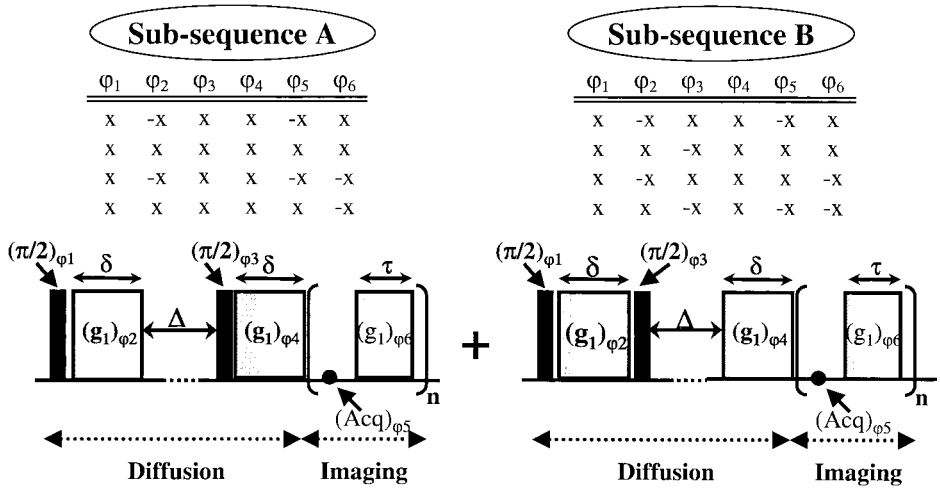

Figure 8 The basic sequence composed of the two subsequences A and B and their associated phase cyclings for providing diffusion weighted images with RF field gradients. The homogeneous $\pi/2$ pulses (black rectangles) inserted in the diffusion contrast period enable one to remove the spatial modulation inherent to the sequence in Figure 7 and to retain only the signal attenuation due to diffusion. The various symbols have the same meaning as in Figure 7.

resolution is even achieved with objects for which severe magnetic susceptibility variations exist and which for that reason require the use of much higher $\mathbf{B}_0$ gradients in conventional imaging.

Although, so far, we have discussed spin density image, the widespread success of NMR imaging also results from the range of contrast available. The fundamental approach for applying contrast is to precondition the magnetization prior the imaging step (Figure 6). Including effects of contrast, Equation 9 can be written:

$$S(t) = \int \rho(X)E(X,t)\sin(\gamma g_1 Xt)dX \qquad (10)$$

where $E(X,t)$ is the normalized contrast factor. Thus image reconstruction returns $\rho(X)E(X,t)$. As in $\mathbf{B}_0$ gradient imaging [8], a whole array of image contrast schemes (e.g., in relaxation times, chemical shift, molecular motion) is now available in $\mathbf{B}_1$ gradient imaging. In addition, two-dimensional maps of the contrast information can be computed from a series of images acquired under different contrast conditions. In particular, high quality maps of longitudinal relaxation time T_1 [23] and diffusion coefficient [59] can be obtained.

Diffusion imaging

The potential of $\mathbf{B}_1$ gradient NMR microscopy is particularly highlighted by some results recently obtained in diffusion imaging. The basic idea for determining spatially resolved diffusion coefficients with RF field gradients is to replace the second gradient pulse and the read pulse in the basic sequence (Figure 4) by a rapid rotating frame imaging sequence (Figure 7). However, this simple method yields one-dimensional profiles whose amplitude is not only a function of the local self-diffusion

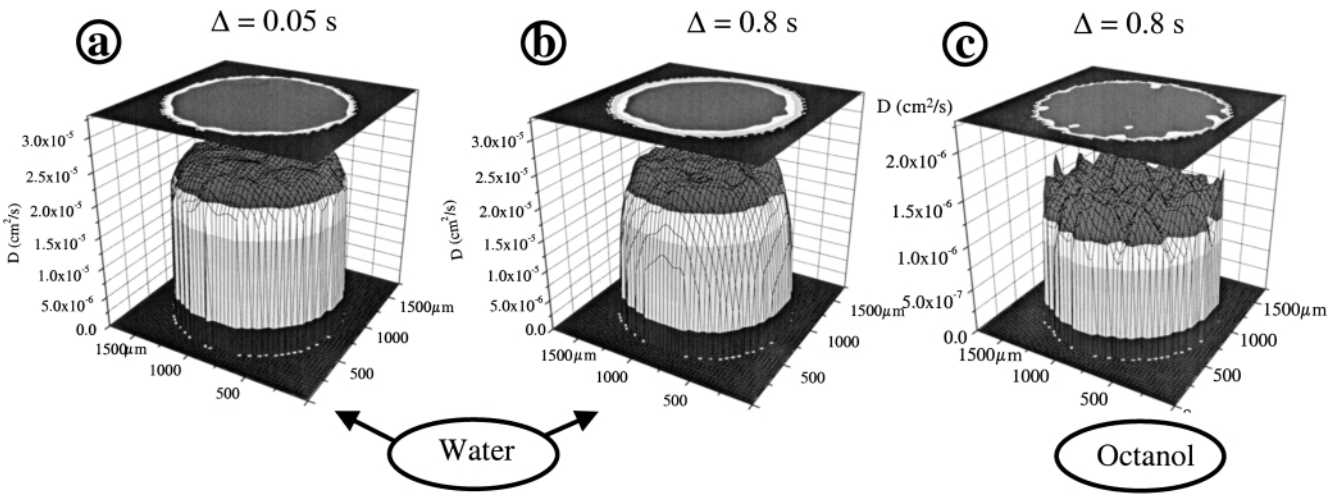

Figure 9 The self-diffusion coefficient maps of two capillaries of 1.3-mm inside diameter filled respectively (a), (b) with water and (c) with octanol. The diffusion times Δ were respectively (a) 0.05 s and (b) 0.8 s. B_0, 2.1 T; gradient strength g_1, 50 G cm^{-1}; angle increment used in the two-dimensional imaging process, 6°; 64 scans for each angle increment; slice thickness, 2 mm; spatial resolution, 11 μm. These maps result from a series of five diffusion-weighted images obtained by using the sequence shown in Figure 8 with (a) δ = 10, 350, 450, 600, 750 μs; (b) δ = 10, 75, 100, 140, 175 μs; (c) δ = 10, 450, 750, 1400, 1750 μs; (d) δ = 10, 100, 250, 400, 500 μs.

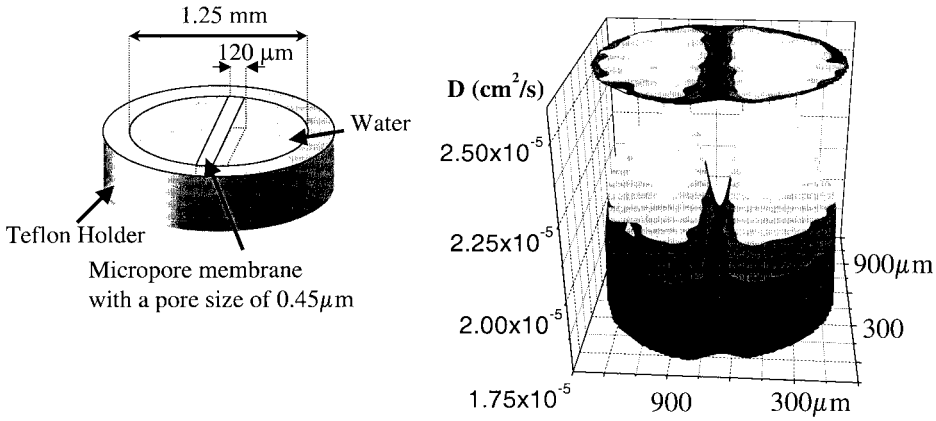

Figure 10 The self-diffusion coefficient map obtained using the sequence in Figure 8 or water outside and inside a Millipore HVLP membrane of 120-μm thickness and with a pore size of 0.45 μm. The membrane of 2-mm height was perfectly fitted into a Teflon cylindrical holder of 1.3-mm inner diameter. The map results from a series of four diffusion-weighted images with, respectively, δ = 290, 500, 650, and 750 μs; B_0, 2.1 T; g_1, 50 G cm^{-1} Δ: 50ms.

coefficient but also is modulated by a cosine function of spatial coordinates. To cancel this modulation and thus to obtain true self-diffusion coefficient maps in a straightforward manner, the more elaborate sequence schematised in Figure 8 is required [59]. Below are presented two examples that will allow the reader to assess the capabilities of the method and to foresee the various possible applications in environmental biotechnology.

Restricted diffusion at solid/liquid interfaces [25]: Figure 9 shows the self-diffusion coefficient maps obtained, respectively for water and octanol capillaries at two different diffusion times Δ by using the sequence in Figure 8. We note that the self-diffusion coefficients measured through the samples are in excellent agreement with the expected values at 25°C ($D_{water}=2.3\times10^{-5}$ cm^2 s^{-1} and $D_{octanol}=1.4\times10^{-6}$ cm^2 s^{-1}) except on the water capillary periphery where the diffusion coefficient value drops continuously as the distance from the wall decreases. This effect, which is more pronounced as the diffusion time Δ or diffusion coefficient D increases, is merely the signature of restricted molecular diffusion in the vicinity of a reflective wall. We have demonstrated that this effect can be relatively well described with a simple one-dimensional model adapted to the situation of molecules close to a reflective wall perpendicular to the gradient direction [25]. This result is very important because it visualizes quantitatively, for the first time in NMR microscopy, the restricted diffusion at a solid/liquid interface. To date, only diffusion-mediated edge spikes have been observed in $\mathbf{B}_0$ gradient NMR imaging [9,45]. This important result must be directly connected with the major advantage of $\mathbf{B}_1$ gradients over $\mathbf{B}_0$ gradients, namely their quasi-immunity to magnetic susceptibility variations occurring in particular at interfaces.

Diffusion through a membrane [59]: The second example is related to the behavior of fluids within porous materials such as membranes. Figure 10 shows the self-diffusion map of water outside and inside a Millipore HVLP membrane of 120-μm thickness and with a pore size of 0.45 μm. The membrane was perfectly fitted into a Teflon cylindrical holder of 1.3-mm inner diameter. As expected, the hindrance encountered by the water molecules inside the membrane lead to diffusion coefficient values that are significantly smaller inside the membrane than outside (about 1.9 10^{-5} cm^2 s^{-1} and 2.3 10^{-5} cm^2 s^{-1}, respectively). In addition, the diffusion coefficient values drop slowly not only in the vicinity of the holder wall, as in Figure 9, but also in the vicinity of the membrane, approximately in a layer of 30-μm thickness on either side of the membrane. It is also interesting to note that the two restriction effects, due to the membrane and to the holder wall, respectively, add up at the ends of the membrane and reinforce the lowering of the localized diffusion coefficients, hence the widening of the isodensity surfaces.

Conclusion and perspectives

The technical and methodological advances made in $\mathbf{B}_1$ gradient NMR microscopy over the last few years have increased significantly the capabilities of this technique, which are now close to those of $\mathbf{B}_0$ gradient NMR microscopy in particular in terms of in-plane spatial resolution (a few micrometers) and measurable diffusion coefficients (down to 10^{-9} cm^2 s^{-1}). In addition, the availability of reliable very high power RF amplifiers (power in the order of 1 kW or more) should allow further improvement. Nevertheless some difficulties remain in particular for creating two or three independent orthogonal $\mathbf{B}_1$ gradients, hence in two-dimensional imaging the necessity of rotating the sample for performing an image. Considering the efficiency and the popularity of $\mathbf{B}_0$ gradients, this assessment could suggest that there is practically no interest in carrying on the development of $\mathbf{B}_1$ gradient NMR microscopy. But that is without taking into consideration the major asset of this technique, namely a quasi-immunity to the background static magnetic field gradients arising from magnetic susceptibility inhomogeneities. Thus, $\mathbf{B}_1$ gradient NMR microscopy should be the method of choice for studying molecular diffusion in heterogeneous media without the necessity of using large gradients as shown by the two diffusion imaging examples reported here. Among the fields that could benefit from this tool, there are, in particular, all those dealing with diffusion processes in environmental science. Indeed, to date, in spite of its noninvasive and nondestructive character, NMR has been little used in this area for diffusion measurements. One of the reasons is directly related to the difficulties encountered by the $\mathbf{B}_0$

gradient technique when background gradients are present. Thus, the diffusion maps presented here are not only academic. In fact, they are the preliminaries to interesting future applications in environmental biotechnology: measuring local flow velocity profiles within a membrane module or a biofilm and detecting the distribution of water channels in the membrane module or the biofilm, monitoring the transmembrane transport of solutes (straightforward or *via* paramagnetic ions), measuring the mobility of different biofilm components (water, polysaccharides, antimicrobial agents) by using NMR spectral editing methods, studying and monitoring sludges dewatering, characterization of floc structure in wastewater treatment, studying fluid mass transfer and transport in soil. Finally, it may be expected that the possibilities of $\mathbf{B}_1$ gradient NMR microscopy would be further increased on the one hand by designing coil or resonator systems for producing strong $\mathbf{B}_1$ gradients at frequencies higher than 300 MHz (the sensitivity but also the background gradient effects increasing with the Larmor frequencies) and on the other hand, by taking advantage of the instrumental simplicity of this technique for developing low-field dedicated spectrometers for performing *in situ* studies, following the approach of Blümich *et al.* for the NMR-MOUSE [5].

References

1 Ackerman JH, TH Grove, GG Wong, DG Gadian and GK Radda. 1980. Mapping of metabolites in whole animals by ^{31}P NMR using surface coils. *Nature* 283: 167–170.
2 De Beer D and P Stooley. 1995. Relation between the structure of an aerobic biofilm and transport phenomena. *Water Sci Technol* 32: 11–18.
3 De Beer D, P Stoodley and Z Lewandowski. 1997. Measurement of local diffusion coefficients in biofilms by microinjection and confocal microscopy. *Biotechnol Bioeng* 53: 151–158.
4 Beuling EE, D van Dusschoten, P Lens, JC van den Heuvel, H Van As and SPP Ottengraf. 1998. Characterization of the diffusive properties of biofilms using pulsed field gradient-nuclear magnetic resonance. *Biotechnol Bioeng* 60: 283–291.
5 Blümich B, P Blümler, G Eidmann, A Guthausen, R Haken, U Schmitz, K Saito and G Zimmer. 1998. The NMR-MOUSE: construction, excitation, and applications. *Magn Reson Imaging* 16: 479–484.
6 Boudot D, D Canet and J Brondeau. 1990. Spatial labeling by a radiofrequency field gradient. DANTE-Z profile, probed by one-dimensional nutation imaging. *J Magn Reson* 87: 385–394.
7 Brito AG and LF Melo. 1999. Mass transfer coefficients within anaerobic biofilms: effects of external liquid velocity. *Water Res* 33: 3673–3678.
8 Callaghan PT. 1993. Principles of Nuclear Magnetic Resonance Microscopy. Oxford Univ. Press, Oxford.
9 Callaghan PT, A Coy, LC Forde and CJ Rofe. 1993. Diffusive relaxation and edge enhancement in NMR microscopy. *J Magn Reson* A 101: 347–350.
10 Canet D, B Diter, A Belmajdoub, J Brondeau, JC Boubel and K Elbayed. 1989. Self-diffusion measurements using a radiofrequency field gradient. *J Magn Reson* 81: 1–12.
11 Chen YM, LM Abriola, PJJ Alvarez, PJ Anid and TM Vogel. 1992. Modeling transport and biodegradation of benzene and toluene in sandy aquifer material: comparisons with experimental measurements. *Water Resour Res* 28: 1833.
12 Dereppe JM, C Moreaux and F Humbert. 1998. NMR diffusion measurements in heterogeneous media using pulsed radio-frequency field gradients. *Microporous Mesoporous Mater* 21: 645–650.
13 Dibiaso D, J Scott, P Harris and S Moore. 1993. The relationship between fluid flow and cell growth in hollow-fiber bioreactors; applications of magnetic resonance imaging. *BHR Group Conf Ser Publ* 5: 457–473.
14 Dupeyre R, Ph Devoulon, D Bourgeois and M Décorps. 1991. Diffusion measurements using stimulated rotary echoes. *J Magn Reson* 95: 589–596.
15 Fan A, P Somasundaran and NJ Turro. 1999. Proton nuclear magnetic resonance study of water in flocs. *Langmuir* 15: 4922–4926.
16 Haase A, C Malloy and GK Radda. 1983. Spatial localization of high resolution ^{31}P spectra with a surface coil. *J Magn Reson* 55: 164–169.
17 Hong X and WT Dixon. 1992. Measuring diffusion in inhomogeneous systems in imaging mode using antisymmetric sensitizing gradients. *J Magn Reson* 99: 561–570.
18 Horsfield MA, SA Clark and TJ Norwood. 1996. Estimation of the characteristic length scales for BO variation using the OE-CTPG pulse sequence. *J Magn Reson A* 122: 222.
19 Hoult DI. 1979. Rotating frame zeugmatography. *J Magn Reson* 33: 183–197.
20 Hoyle BL and P Baveye. 1999. Transport of organic xenobiotics in environment. In: Baveye P *et al.* (Ed.), Bioavailability of Organic Xenobiotics in the Environment. Kluwer Academic Publishers, Dordrecht, pp. 381–405.
21 Humbert F, B Diter and D Canet. 1996. NMR Microscopy by strong radiofrequency-field gradients with spatial resolution better than five micrometers. *J Magn Reson A* 123: 242–245.
22 Humbert F, B Diter, M Valtier, A Retournard and D Canet. 1999. Recent progress in NMR microscopy using B_1 gradients. Abstracts of the 5th international Conference on Magnetic Resonance Microscopy: Heidelberg, Germany, Sept 5–9: 08 p. 89.
23 Humbert F, E Collenne, M Valtier and D Canet. 1999. Nuclear longitudinal relaxation time images by radio-frequency field gradients. *J Magn Reson* 138: 164–166.
24 Humbert F, M Valtier, A Retournard and D Canet. 1998. Diffusion measurements using radiofrequency field gradient: artifacts, remedies, practical hints. *J Magn Reson* 134: 245–254.
25 Humbert F, M Valtier and D Canet. 1999. Restricted molecular diffusion in the vicinity of a reflective wall as probed by NMR measurements using radio-frequency field gradients. *Chem Phys Lett* 302: 1–6.
26 Hürlimann MD. 1998. Effective gradients in porous media due to susceptibility differences. *J Magn Reson* 131: 232–240.
27 Jardine PM, SE Fendorf, MA Mayes, IL Larsen, SC Brooks and WB Bailey. 1999. Fate and transport of hexavalent chromium in undisturbed heterogeneous soil. *Environ Sci Technol* 33: 2939–2944.
28 Karczmar GS, DB Twieg, TJ Lawry, GB Matson and MW Weiner. 1988. Detection of motion using B1 gradients. *Magn Reson Med* 7: 111–116.
29 Karlicek RF and IJ Lowe. 1980. A modified pulsed gradient technique for measuring diffusion in the presence of large background gradients. *J Magn Reson* 37: 75–91.
30 Khandelwal A, AJ Rabideau and P Shen. 1998. Analysis of diffusion and sorption of organic solutes in soil–bentonite barrier materials. *Environ Sci Technol* 32: 1333–1339.
31 Kinchesh P, EW Randall and K Zick. 1992. The elimination of magnetic susceptibility distortions in the imaging of liquids in solids: the stray field imaging technique. *J Magn Reson* 100: 411.
32 La Heij EJ, PJAM Kerkhof, K Kopinga and L Pel. 1996. Determination porosity profiles during filtration and expression of sewage sludge by NMR imaging. *AICHE J* 42: 953–959.
33 Latour LL, L Li and CH Sotak. 1993. Improved PFG stimulated-echo method for the measurement of diffusion in inhomogeneous fields. *J Magn Reson B* 101: 72–77.
34 Latour LL, PP Mitra, RL Kleinberg and CH Sotak. 1993. Time-dependent diffusion coefficient of fluids in porous media as a probe of surface-to-volume ratio. *J Magn Reson A* 101: 342–346.
35 Le Bihan D. 1995. Molecular diffusion, tissue microdynamics and microstructure. *NMR Biomed* 8: 375.
36 Lens P, L Hulshoff Pol, G Lettinga and H Van As. 1997. Use of ^{1}H NMR to study transport processes in sulfidogenic granular sludge. *Water Sci Technol* 36: 157–163.
37 Lewandowski Z, SA Altobelli and E Fukushima. 1993. NMR and microelectrode studies of hydrodynamics and kinetics in biofilms. *Biotechnol Prog* 9: 40–45.
38 Lewandowski Z, SA Altobelli, PD Majors and E Fukushima. 1992. NMR imaging of hydrodynamics near microbially colonized surfaces. *Water Sci Technol* 26: 577–584.
39 Lian J, DS Williams and IJ Lowe. 1994. Magnetic resonance imaging of diffusion in the presence of background gradients and imaging of background gradients. *J Magn Reson A* 106: 65–74.

40 Nakashima Y, F Mitsumori, S Nakashima and M Takahashi. 1999. Measurement of self-diffusion coefficients of water in smectite by stimulated echo 1H nuclear magnetic resonance imaging. *Appl Clay Sc* 14: 59–68.
41 Nestle N and R Kimmich. 1996. Heavy metal uptake of alginate gels studied by NMR microscopy. *Colloids Surf A* 115: 141–147.
42 Pfeuffer J, U Flögel, W Dreher and D Leibfritz. 1998. Restricted diffusion and exchange of intracellular water: theoretical modelling and diffusion time dependence of 1H NMR measurements on perfused glial cells. *NMR Biomed* 11: 19.
43 Potter K, RL Kleinberg, FJ Brockman and EW McFarland. 1996. Assay for bacteria in porous media by diffusion-weighted NMR. *J Magn Reson* 113B: 9–15.
44 Price WS. 1997. Pulsed-field gradient nuclear magnetic resonance as a tool for studying translational diffusion: Part 1. Basic theory. *Concepts Magn Reson* 9: 299–336.
45 Pütz B, D Barsky and K Schulten. 1992. Edge enhancement by diffusion in microscopic magnetic resonance imaging. *J Magn Reson* 97: 27–53.
46 Raulet R, JM Escanyé, F Humbert and D Canet. 1996. Quasi-immunity of B1 gradient NMR microscopy to magnetic susceptibility. *J Magn Reson A* 119: 111.
47 Reeves AD and JA Chudek. 1998. Application of nuclear magnetic resonance imaging (MRI) to migration studies of oil-related residues in estuarine sediments (Tay estuary). *Water Sci Technol* 38: 187–192.
48 Rofe CF, J van Noort, PJ Back and PT Callaghan. 1995. NMR Microscopy using large, pulsed magnetic field gradients. *J Magn Reson B* 108: 125–136.
49 Salmon PM, SB Libicki and CR Robertson. 1988. A theoretical investigation of convective transport in the hollow-fiber reactor. *Chem Eng Commun* 66: 221–247.
50 Schmitt and HC Flemming. 1999. Water binding in biofilms. *Water Sci Technol* 39: 77–82.
51 Shackelford CD. 1991. Laboratory diffusion testing for waste disposal — a review. *J Contam Hydrol* 7: 177–217.
52 Solomon I. 1959. Rotary spin echoes. *Phys Rev Lett* 2: 301.
53 Stejskal EO and JE Tanner. 1965. Spin diffusion measurements: spin echoes in the presence of a time-dependent field gradient. *J Chem Phys* 42: 288–292.
54 Suci PA, JD Vrany and MW Mittelman. 1998. Investigation of interactions between antimicrobial agents and bacterial biofilms using attenuated total reflection Fourier transform infrared spectroscopy. *Biomaterials* 19: 327–339.
55 Tallarek U, D van Dusschoten, H Van As, G Guiochon and E Bayer. 1998. Direct observation of fluid mass transfer resistance in porous media by NMR spectroscopy. *Angew Chem Int Ed* 37: 1882–1885.
56 Thomsen AB, K Henriksen, C Gron and P Moldrup. 1999. Sorption, transport and degradation of quinoline in unsaturated soil. *Environ Sci Technol* 33: 2891–2898.
57 Van As H and D van Dusschoten. 1997. NMR methods for imaging of transport processes in micro-porous systems. *Geoderma* 80: 389–403.
58 van Dusschoten D, PA de Jager and H Van As. 1995. Flexible PFG NMR Desensitized for susceptibility artifacts, using the PFG multiple-spin-echo sequence. *J Magn Reson A* 112: 237–240.
59 Valtier M, F Humbert and D Canet. 1999. Maps of self-diffusion coefficients by radiofrequency field gradient NMR microscopy. *J Magn Reson* 141: 7–17.
60 Vogt M, HC Flemming and WS Veeman. 2000. Diffusion in Pseudomonas biofilms: a pulsed field gradient NMR study. *J Biotechnol* 77: 137–146.
61 Xia F, H Beyenal and Z Lewandowski. 1998. An electrochemical technique to measure local flow velocity in biofilms. *Water Res* 32: 3631–3636.